



Investigation of the effect of light on the electrical parameters of Si/TiO₂ heterojunctions produced by anodic oxidation on p-type Si wafer

Fatih Unal^{1,*} , Mustafa Sükrü Kurt², and Salih Durdu³

¹Central Research Laboratories GRUMLAB, Giresun University, 28200 Giresun, Turkey

²Department of Physics, Erzurum Technical University, Erzurum, Turkey

³Industrial Engineering, Giresun University, 28200 Giresun, Turkey

Received: 12 April 2022

Accepted: 26 May 2022

Published online:

7 June 2022

© The Author(s), under exclusive licence to Springer Science+Business Media, LLC, part of Springer Nature 2022

ABSTRACT

Fabrication of heterojunctions of Si combined with TiO₂ oxide-based semiconductors is an alternative method to produce cost effective photodiodes at last decade. In this study, to investigate the photodiode parameters of the p-type Si/TiO₂ heterojunctions, TiO₂ films were coated on the p-type Si wafer surface by combined magnetron sputter (PVD) and anodic oxidation methods. Surface morphology and elemental distributions of Si/TiO₂ heterojunctions were performed by SEM and EDS-mapping, respectively. The surfaces were rough and the roughness values increased with the increase of the anodic oxidation voltage. The titanium and oxygen elements were homogenously distributed through the whole surfaces. The electrical characterization of heterojunctions produced with different voltage values was investigated in the ± 5 V potential range under dark and 40, 60, 140, 190, 290 and 420 W m⁻² light intensity. All heterojunctions showed rectifying properties and exhibited typical photodiode behavior sensitive to light. Series resistance (R_s), shunt resistance (R_{sh}), diode ideality factor (n), barrier height (ϕ_b) and reverse saturation current (I_0) values of heterojunctions were investigated under different light intensities. Under dark and 420 W m⁻² light intensity, the lowest R_s and R_{sh} values (calculated from Ohm's law) were found to be 146–122 Ω and 1308–795 Ω for the heterojunction produced at 20 V, respectively, while the lowest n values (calculated from Cheung&Cheung method) were between 1.779 and 1.825. Moreover, ϕ_b values (calculated from Cheung&Cheung method) are measured between 0.215 and 0.378 eV, while I_0 values (calculated from conventional method) in the dark environment are between 3.26×10^{-7} and 2.99×10^{-4} A.

Address correspondence to E-mail: fatih.unal@giresun.edu.tr

1 Introduction

Despite fast technological advancements, fossil fuels seem to be favored as energy sources with considerable utilization potential. In this regard, it is critical for nanotechnology to produce environmentally friendly devices. Due to their high efficiency, ease of manufacture, and good electrical properties, photodiodes, and photovoltaics are extremely important as an environmentally friendly solution to energy problems [1, 2]. To improve the opto-electronic and electrical properties of photodiodes in thin-film technologies, various techniques such as spin coating, electrochemical deposition, epitaxial growth, and magnetron sputtering are mostly preferred to grow thin films [3, 4]. Among these techniques, magnetron sputtering provides some advantages, including the ability to grow ultra-thin samples in a controlled manner and high flux rates. Electrochemical deposition techniques are also widely used due to their low cost and easy implementation.

Earlier, the electrical properties of organic [rubrene, coronene, CuPc, PMltz, Poly (3-hexylthiophene) etc.] and inorganic (InSe, ZnO, CIGS etc.) materials have been investigated in detail [5–9]. Inorganic materials are less durable and unstable since they are easily affected by external factors including mechanical stress, light, and humidity. On the other hand, the electric and opto-electronic properties of metallic thin films have been well defined, which are also more durable and stable. Therefore, they are not easily affected by external factors [10, 11]. Because of such properties, metal oxide films are widely used in photodetector and photodiode applications. Metal oxides such as AlO, BiO, CdO, ZnO, NiO, and TiO₂ have been mostly used in these applications.

TiO₂ draws considerable attention among these materials owing to its unique functional properties, which include mechanical, chemical, electronic, and optical properties. It is widely used in a variety of applications, such as anti-bacterial coatings, humidity and gas detectors, energy storage, photocatalysis, photovoltaic panels, etc. [12–14]. TiO₂ is also remarkable for its high absorbance and low bandgap energy, as well as its photoresponse and photovoltaic properties as investigated previously [15–17].

There are some reports on fabrication and characterization of Si wafer/TiO₂ films by e-beam, dip coating, sol-gel, pulsed laser deposition etc. in the

literature. Rawat et al. produced e-beam evaporated n-TiO₂ capped p-Si nanowires heterojunction and investigated electrical and ultraviolet-A detection properties [18]. Rawat et al. produced e-beam evaporated p-Si/n-TiO₂ heterojunction and evaluated ultraviolet detection properties [19]. Sani analyzed opto-electronic properties of TiO₂ nanowires/Si heterojunction arrays [20]. Kumbhar et al. investigated dip coated TiO₂ based metal–semiconductor–metal ultraviolet photodetector for UV A monitoring [21]. Kumar et al. evaluated structural and electrical properties of Ag/n-TiO₂/p-Si/Al heterostructure fabricated by pulsed laser deposition technique [22]. However, there is no report on the fabrication and characterization of p-Si/TiO₂ by magnetron sputter and anodic oxidation in the literature. Thus, unlike the literature, a Ti layer was deposited on p-type Si substrates using the magnetron sputtering technique. And then, Ti layer was oxidized to TiO₂ layer at various voltages by anodic oxidation process. To present alternative for opto-electronic, electrical properties such as R_s , R_{sh} , n , ϕ_b and I_0 of different Si/TiO₂ heterojunctions were characterized by using various methods such as conventional and Cheung&Cheung. The morphology, elemental distribution and opto-electronic properties of Al/Si/TiO₂/Ag heterojunctions produced at different anodic oxidation voltages (10 V, 15 V, and 20 V) were investigated by SEM, EDS-mapping and I - V measurements under various light intensities, respectively.

2 Experimental details

2.1 PVD sputter process

In advance for the sputtering process, the p-type Si substrates were cleaned for 5 min with acetone, methanol, and distilled water using an ultrasonic cleaner, and then the cleaning process was completed with nitrogen blow-drying. Samples were prepared using 2-inch diameter Ti solid targets with 99.99% purity. Before starting the coating Ti, a plasma cleaning process was applied to Ti target for 10 min to increase surface activity and clean the surface area. All samples were coated using a sputtering system of the Nanovak brand and NVTS-400 model. During the Ti coating process of the samples, the base pressure was around 4.1×10^{-6} mTorr, while the working

pressure was around 3.45×10^{-3} mTorr in the Ar gas environment. A quartz thickness monitor was used to determine the sample deposition rates. Ti was deposited on a substrate with deposition rates of 0.8 \AA s^{-1} (430 V/120 mA DC power). The distance between the substrate and the target was about 15 cm, and the temperature was around 25 °C. The coating process was completed by coating the Si substrates with 1 μm Ti. To form ohmic contact, Al layer was deposited on p-type Si wafer (opposite direction of Ti layer). And then, Al layer was annealed under vacuum conditions in sputter chamber.

2.2 Anodic oxidation process

A DC (direct current) power supply was used to produce TiO_2 layer. The Ti-coated p-type semiconductor substrate served as an anode while a Pt sheet was used as a cathode through oxidation process. The electrolyte was prepared by dissolving NH_4F and deionized water into $\text{C}_2\text{H}_6\text{O}_2$. The electrolyte temperature was kept below 30 °C through process. The oxidation process was carried out at different voltage values (10, 15, and 20 V) under a constant current (0.02 A) for 60 min. After the oxidation process, they were cleaned in an ultrasonic bath and dried with hot air. To form rectifier contact, Ag dots was deposited on TiO_2 layer by PVD.

2.3 Surface characterization

The surface morphologies and elemental distribution of the samples were investigated by SEM (Hitachi SU1510) and EDS attached to SEM, respectively. Roughness values was calculated from SEM images by Gwyddion software.

2.4 Electrical characterization

The electrical characterization of heterojunctions produced at different voltages was investigated in the ± 5 V potential range under dark and 40, 60, 140, 190, 290, and 420 W m^{-2} light intensity by solar simulator system (SCIENCETECH Solar Simulator System AAA model).

3 Results and discussion

3.1 Surface analyses

Surface morphologies of the oxidized Ti layers produced at 10, 15, and 20 V were illustrated in Fig. 1a–c, respectively. The surface becomes rough and porous with increasing potential, as seen in Fig. 1a–c. Ti layer ionize positively-charged Ti^{4+} ions after the process began. Simultaneously, positively-charged Ti^{4+} ions and negatively-charged OH^- ions react with each other under constant voltage by the interaction of opposite charged ions. Eventually, oxidized Ti layer forms on p-type semiconductor as seen in Fig. 1. With increasing voltage, more and more opposite charged ions migrate on the surface. Finally, rough oxide surface forms on p-type semiconductor. Average roughness (Ra) of heterojunctions 1st, 2nd and 3rd was calculated as 59.4, 65.0, and 75.0 nm, respectively.

The EDS-mapping analysis images of TiO_2 layers grown on Si layer at different voltages are given in Fig. 2. Only, oxygen and titanium were detected through the whole surfaced as expected. These elements were homogeneously dispersed during films as shown in Fig. 2. The oxygen comes from anodic

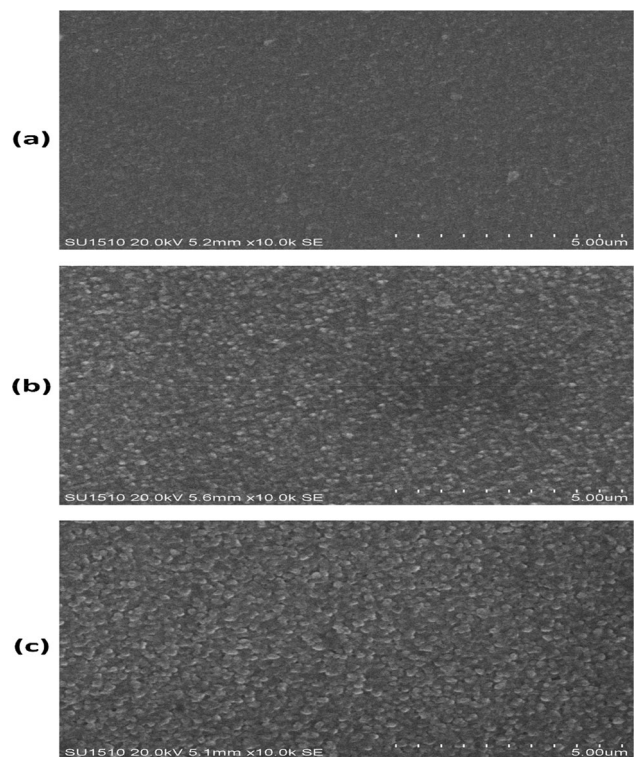


Fig. 1 Surface morphologies of TiO_2 layer: **a** 1st, **b** 2nd and **c** 3rd

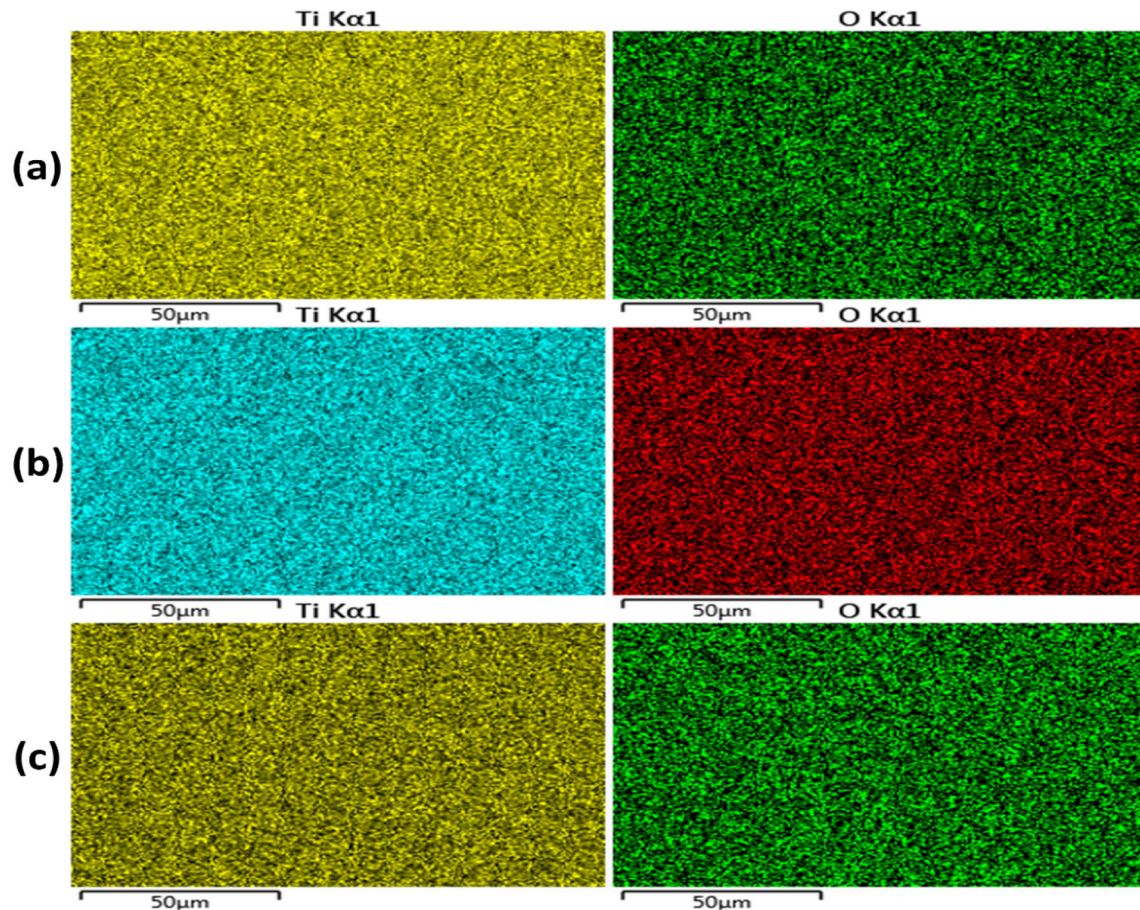


Fig. 2 EDS analyses of TiO₂ layer: **a** 1st, **b** 2nd and **c** 3rd

oxidized TiO₂ layer while the titanium originates in sputter layer and oxidized layer. It could be clearly concluded that all surfaces were chemically homogenous.

3.2 Electrical analyses

3.2.1 *I–V* measurement of Al/Si/TiO₂/Ag

The variation of current versus voltage can be used to determine the basic structure and electrical properties of heterojunctions. Temperature-related current–voltage changes were examined in the literature, as well as at radiation dose and at different light intensities [22–27]. In this study, current–voltage changes of Al/Si/TiO₂/Ag heterojunctions were investigated dark and at 40–420 W m^{−2} light intensities.

I–V graphs of Al/Si/TiO₂/Ag heterojunctions obtained with TiO₂ grown on Si substrate with different oxidation voltage in Fig. 3a–c, and semi-

logarithmic *I–V* graphics of these heterojunctions in Fig. 4a–c. As can be seen in Fig. 3a–c, it showed rectifying characteristic at three heterojunctions. The electrical conductivity specifically increased with increasing light intensity under forward bias as shown in Fig. 3a.

Figure 4a–c shows an asymmetry under forward and reverse bias. The linear region corresponds to 0–0.94 V at the 1st heterojunction, 0–0.38 V at the 2nd heterojunction, and 0–0.48 V at the 3rd heterojunction under forward bias conditions. Above these voltage values, the effect of series resistance occurs and linearity disappears. In reverse bias conditions, there is non-saturation in all three heterojunctions. This situation is caused by the interfacial barrier height between the TiO₂ layer and the Ag metal reducing the image charge forces [28–30]. In all heterojunctions, conductivity increases with increasing light intensity. The photons have energy higher than the forbidden band gap cause to form new electron–hole pairs in the depletion region. The structure stressed

Fig. 3 I–V graph of heterojunction: a 1st, b 2nd and c 3rd

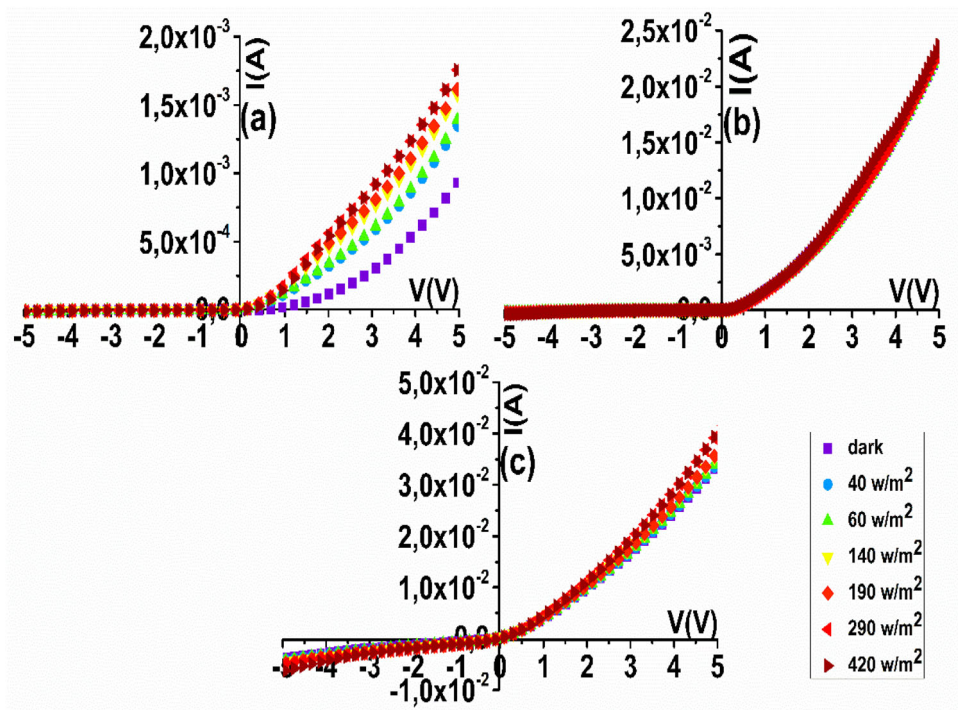
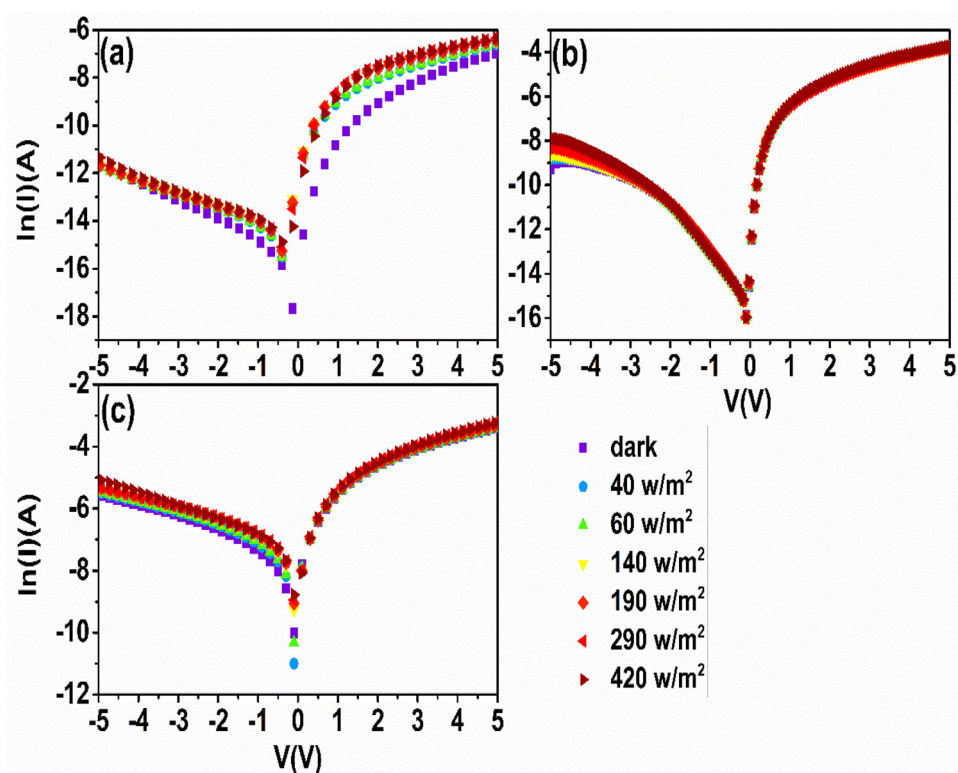


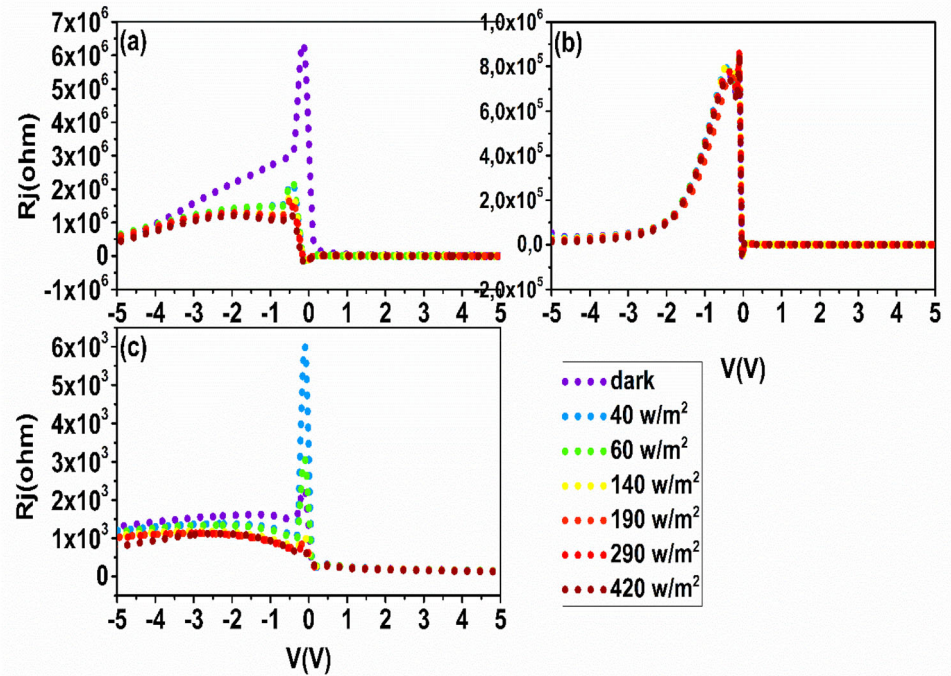
Fig. 4 Semi-logarithmic I–V graph of heterojunction: a 1st, b 2nd and c 3rd



under the external electric field creates a strong internal electric field at the grain boundaries. This internal electric field separates the newly formed electron–hole pairs. The holes slowly act compared to

electrons while the electrons were quickly swept. As a result of these, the current rises. This is the basis of photoconductivity.

Fig. 5 R_j - V graph of heterojunction: a 1st, b 2nd and c 3rd



In Fig. 5a–c, graphs of heterojunctions for R_j - V are given. Series and shunt resistances are important parameters for the quality and performance of diodes [31]. High R_{sh} and low R_s values provide performance in diodes. R_s and R_{sh} values can be calculated from the graph of the junction resistance $R_j = \frac{dV}{dI}$ versus V . The constant value in the lower region corresponds to R_s under forward bias while the constant value in the lower region corresponds to R_{sh} under reverse bias. R_s is in series with the photocurrent source while R_{sh} is in parallel with the photocurrent source [32]. There are several factors that cause the series resistance R_s in a diode. The first factor is the movement of current through the emitter and the base of the diode. The second factor is the resistance formed between Si and TiO_2 and the resistance formed in the upper and lower contacts [33]. R_s have some problems especially in high current regions. The main effect of the series resistor is to reduce the fill factor (FF). But extremely high values can also reduce the short-circuit current (I_{sc}). In Tables 1, 2 and 3, the R_s and R_{sh} values obtained from the R_j - V graph of all three heterojunctions under different light intensity are given. The R_s values of the 1st, 2nd and 3rd heterojunction under dark and 420 W m^{-2} light intensity were approximately measured as $4.962 \times 10^3 \text{ } \Omega$ to $2.673 \times 10^3 \text{ } \Omega$, $0.219 \times 10^3 \text{ } \Omega$ to $0.213 \times 10^3 \text{ } \Omega$, and $0.146 \times 10^3 \text{ } \Omega$ to $0.122 \times 10^3 \text{ } \Omega$

Ω , respectively. Similarly, The R_{sh} values of the 1st, 2nd and 3rd heterojunction under dark and 420 W/m^2 light intensity were approximately measured as $5.057 \times 10^5 \text{ } \Omega$ to $4.184 \times 10^5 \text{ } \Omega$, $5.305 \times 10^4 \text{ } \Omega$ to $1.341 \times 10^4 \text{ } \Omega$, and $1.308 \times 10^3 \text{ } \Omega$ to $0.795 \times 10^3 \text{ } \Omega$, respectively. It was clearly observed that both R_s and R_{sh} values decreased with increasing light intensity. The increase in applied potential in anodic oxidation caused a decrease in R_s and R_{sh} values. As seen in the SEM images; with increasing voltage, films with larger particle sizes are formed and the surface roughness increases. Increasing the particle size reduces the dispersion at the grain boundaries and undesirable quantum mechanical states are eliminated. In addition, more regular structures have fewer defects [8]. As a result, all of these caused to decrease the R_s and R_{sh} values with increasing light intensity.

3.2.2 Diode parameters of Al/Si/TiO₂/Ag heterojunction

Based on current–voltage data and using different methods, parameters such as diode ideality factor, barrier height, reverse saturation current and series resistance of these diodes can be calculated.

In the traditional method, the relationship between current and voltage is determined according to thermionic emission theory. Equation 1 [7, 26] is below:

$$I = AA^*T^2 \exp\left(-\frac{q\phi_b}{kT}\right) \left[\exp\left(\frac{q(V - IR_s)}{kT}\right) - 1 \right] \quad (1)$$

Here, A is the active diode area, A^* is the Richardson constant (the theoretical Richardson constant for TiO_2 is $1200 \text{ A cm}^{-1} \text{ K}^2$), q is the charge of the electron, ϕ_b is the effective barrier height, k is the boltzman constant, T is the temperature in kelvin, V is the applied potential, R_s is the series resistance.

Equation 1 when $V - IR_s \gg 3kT$

$$I = I_0 \exp\left(\frac{qV}{nkT}\right) \quad (2)$$

$$I_0 = AA^*T^2 \exp\left(-\frac{q\phi_b}{kT}\right) \quad (3)$$

Equation 4 is obtained if the derivative with respect to V is taken after taking the logarithm of Eq. 2.

$$n = \frac{q}{kT} \frac{d(V)}{d(\ln(I))} \quad (4)$$

If the slope of the linear region of the graph of $\ln I$ against V in the low and medium voltage region is calculated together with other constants, the ideality factor n is found. The point where the linear region of the graph of $\ln I$ against V intersects $\ln I$ gives us the reverse saturation current, I_0 . In the traditional method, also the barrier height, ϕ_b is determined from Eq. 3.

In the Cheung and Cheung method, the diode ideality factor, barrier height and series resistance R_s value are determined by using the Cheung and Cheung functions [34]. Cheung and Cheung functions are given in Eqs. 5–7.

$$\frac{dV}{d \ln(I)} = IR_s + \frac{nkT}{q} \quad (5)$$

$$H(I) = V - \frac{nkT}{q} \ln\left(\frac{I}{AA^*T^2}\right) \quad (6)$$

$$H(I) = IR_s + n\phi_b \quad (7)$$

In the equations above, the graph of $dV/d \ln I$ and HI against I is drawn using the values in the low and medium voltage region of the I – V graph. The ideality factor n is calculated by using the slope R_s value of $d(V)/d(\ln(I))$ against I , and the value of the curve intersecting the y -axis by using other constants. ϕ_b is determined by using the n value from the point where the curve cuts the y -axis in the graph drawn by $H(I)$ against I . The slope of this curve gives the

value of R_s . Figures 6a–c and 7a–c show, respectively, the graphs of heterojunctions $d(V)/d(\ln(I))$ against I and the graphs of $H(I)$ against I . It can be clearly seen that both graphs are linear.

R_s , R_{sh} , n , ϕ_b and I_0 values obtained from $\ln(I)$ – V , $d(V)/d(\ln(I))$ and $H(I)$ – I graphs were separately calculated for each heterojunction. R_s , R_{sh} , n , ϕ_b , I_0 values of 1st, 2nd and 3rd heterojunctions under different light intensity are given in Tables 1, 2 and 3, respectively.

Rectifying ratio ($RR = I_{\text{forward}}/I_{\text{reverse}}$) values of all samples were calculated at $\pm 5 \text{ V}$ and the result were given in Table 4. The RR values of 1st and 2nd samples are reasonable with other literature studies. Rawat et al. produced e-beam evaporated n-TiO₂ capped p-Si nanowires heterojunction and RR value was measured as ≈ 75 at 5 V for this sample [18]. Rawat et al. produced e-beam evaporated p-Si/n-TiO₂ heterojunction and RR value was measured as ≈ 30 at 5 V for this sample [19]. However, calculated RR values for 3rd sample is low. Compared to the 1st and 2nd samples, the barrier height value of the 3rd sample is low as the reverse saturation current value of it is high. A low barrier height which causes a high current under reverse bias may lead to reduce the RR value.

The variation of R_s values depending on the light intensity and the variation of R_{sh} are given in Figs. 8a–c and 9a–c, respectively.

It is clearly seen in Fig. 8a–c that the variation of R_s values calculated with different methods versus light intensity exhibits a similar trend. R_s values generally decrease with increasing light intensity in all three heterojunctions. The reason for this decrease is the increase in photoconductivity with increasing light intensity [33]. A similar situation is also seen in the variation of R_{sh} depending on the light intensity in Fig. 9a–c. R_{sh} value in all three heterojunctions decreased with increasing light intensity.

The change of reverse saturation current (I_0) depending on the light intensity of the three heterojunctions is given in Fig. 10a–c. I_0 values of all three heterojunctions exhibit different behavior with light intensity. At the 1st heterojunction, the I_0 value increased up to 140 W m^{-2} light intensity and then, it decreased. At the 2nd heterojunction, the I_0 value increased almost linearly with the increase of light intensity. At the 3rd heterojunction, the I_0 value decreased exponentially up to 290 W m^{-2} and then, it decreased linearly. The reason of I_0 values increase

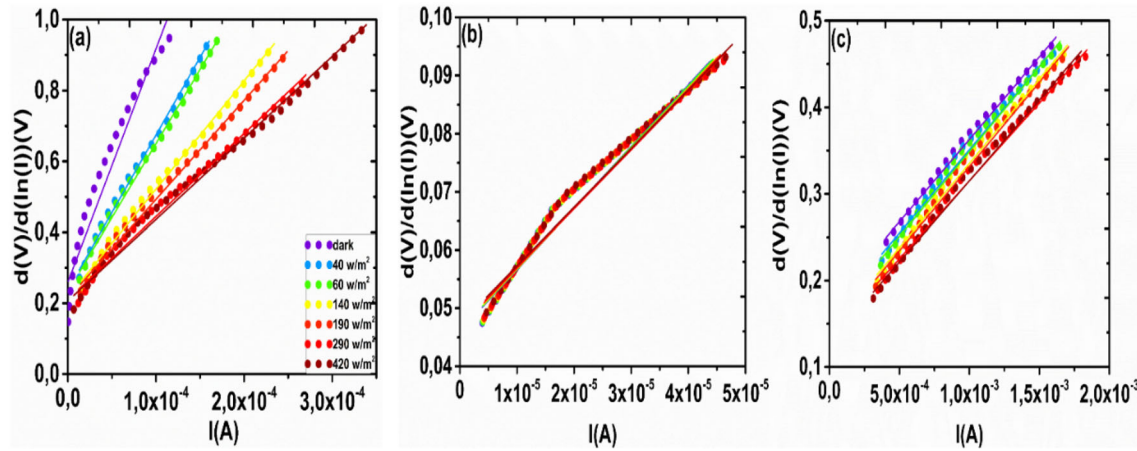


Fig. 6 $d(V)/d(\ln(I))-I$ graph of heterojunction no: a 1st, b 2nd and c 3rd

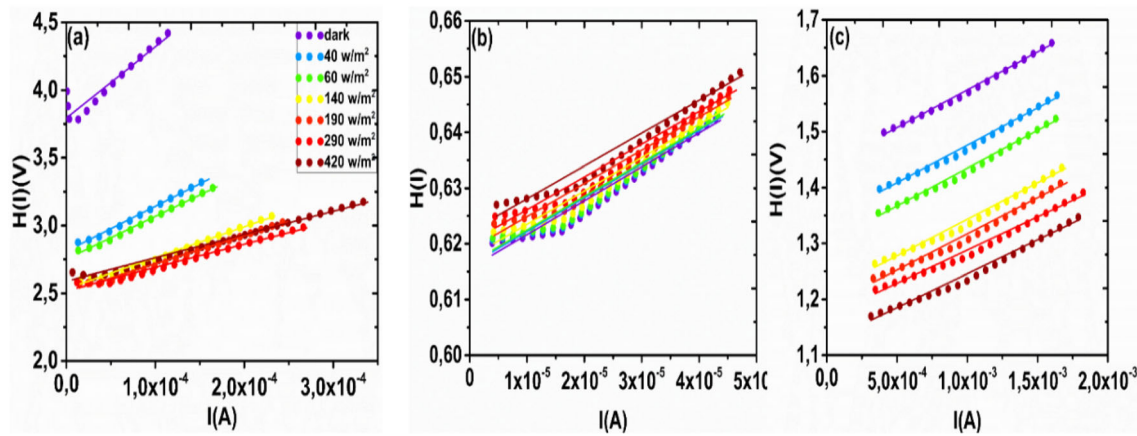


Fig. 7 $H(I)-I$ graph of heterojunction no: a 1st, b 2nd and c 3rd

Table 1 n , R_s , R_{sh} , ϕ_b and I_0 values of heterojunction no. 1

Light intensity ($W\ m^{-2}$)	Rj-V		$dV/d(\ln(I))-I$			$H(I)-I$		$\ln(I)-V$	
	R_s (Ω)	R_{sh} (Ω)	Diode ideality factor (n)	R_s (Ω)	Barrier height ϕ_b (eV)	R_s (Ω)	Diode ideality factor (n)	Barrier height ϕ_b (eV)	Reverse saturation current I_0 (A)
Dark	4962	505,754	10.026	6580	0.378	5250	11.120	0.732	3.26×10^{-7}
40	3505	548,499	9.181	4370	0.306	3325	10.507	0.656	1.04×10^{-5}
60	3402	618,516	8.999	4175	0.305	3167	10.285	0.655	1.06×10^{-5}
140	3078	503,950	8.370	3050	0.302	2283	9.169	0.651	1.22×10^{-5}
190	3001	574,999	8.238	2797	0.304	2074	8.648	0.653	1.15×10^{-5}
290	2799	467,248	8.129	2343	0.310	1707	7.741	0.658	9.27×10^{-6}
420	2673	418,445	7.984	2298	0.324	1719	7.047	0.674	4.99×10^{-6}

with the light intensity is that the illumination activates the interface recombination of photo-generated

carriers [35, 36]. Therefore, it could be stated that the decrease in I_0 values may be related to increase in the

Table 2 n , R_s , R_{sh} , ϕ_b and I_0 values of heterojunction no. 2

Light intensity (W m ⁻²)	Rj-V		dV/d(ln(I)-I)		H(I)-I		ln(I)-V		
	R_s (Ω)	R_{sh} (Ω)	Diode ideality factor (n)	R_s (Ω)	Barrier height ϕ_b (eV)	R_s (Ω)	Diode ideality factor (n)	Barrier height ϕ_b (eV)	Reverse saturation current I_0 (A)
Dark	219.25	53,056	1.779	1059	0.345	607	2147	0.695	2.27×10^{-6}
40	219.44	33,980	1.783	1054	0.345	605	2154	0.694	2.31×10^{-6}
60	219.64	26,698	1.785	1051	0.345	604	2158	0.694	2.33×10^{-6}
140	218.67	28,460	1.793	1038	0.344	598	2170	0.693	2.41×10^{-6}
190	217.03	20,443	1.801	1029	0.343	595	2183	0.692	2.48×10^{-6}
290	217.32	20,147	1.810	1014	0.342	587	2197	0.691	2.58×10^{-6}
420	213.55	13,416	1.825	1009	0.340	588	2227	0.690	2.75×10^{-6}

Table 3 n , R_s , R_{sh} , ϕ_b and I_0 values of heterojunction no. 3

Light intensity (W m ⁻²)	Rj-V		dV/d(ln(I)-I)		H(I)-I		ln(I)-V		
	R_s (Ω)	R_{sh} (Ω)	Diode ideality factor (n)	R_s (Ω)	Barrier height ϕ_b (eV)	R_s (Ω)	Diode ideality factor (n)	Barrier height ϕ_b (eV)	Reverse saturation current I_0 (A)
Dark	146	1308	6.675	190	0.215	135	11.229	0.569	2.99×10^{-4}
40	144	1200	6.134	192	0.218	133	10.530	0.571	2.73×10^{-4}
60	142	1168	5.914	195	0.219	134	10.330	0.572	2.66×10^{-4}
140	137	1072	5.438	194	0.222	130	9.672	0.574	2.44×10^{-4}
190	135	1031	5.297	194	0.224	129	9.459	0.575	2.35×10^{-4}
290	123	1002	5.231	179	0.223	118	9.292	0.574	2.44×10^{-4}
420	122	795	4.950	187	0.227	121	8.895	0.577	2.19×10^{-4}

Table 4 RR values of heterojunction at ± 5 V: (a) 1st, (b) 2nd and (c) 3rd

Samples	RR($I_{forward}/I_{reverse}$)						
	Dark	40 W m ⁻²	60 W m ⁻²	140 W m ⁻²	190 W m ⁻²	290 W m ⁻²	420 W m ⁻²
1st	94.77517	149.1281	173.1472	159.3443	187.5994	164.678	147.4777
2st	244.6451	156.6154	122.9999	131.5153	95.00168	93.66436	63.58264
3st	8.74813	8.142202	8.01559	7.673511	7.433071	7.889943	6.254111

barrier height of 1st heterojunction as shown in Fig. 10a.

The graphs of change of n and ϕ_b values versus to light intensity of all heterojunctions are given in Figs. 11 and 12, respectively. While n values in the first and third heterojunctions decreased with increasing light intensity, ϕ_b values increased. However, the opposite situation was observed in the

second heterojunction. This situation has also been found in some studies [35–37]. The change in n and ϕ_b values with light intensity is the formation and separation of electron-hole pairs, the restructuring and arrangement of molecules on the surface [38]. The n value of ideal diodes is one ($n = 1$) [29]. However, this value could not be reached in all three heterojunctions in this study. There are several

Fig. 8 Variation of R_s values of heterojunction no: a 1st, b 2nd and c 3rd

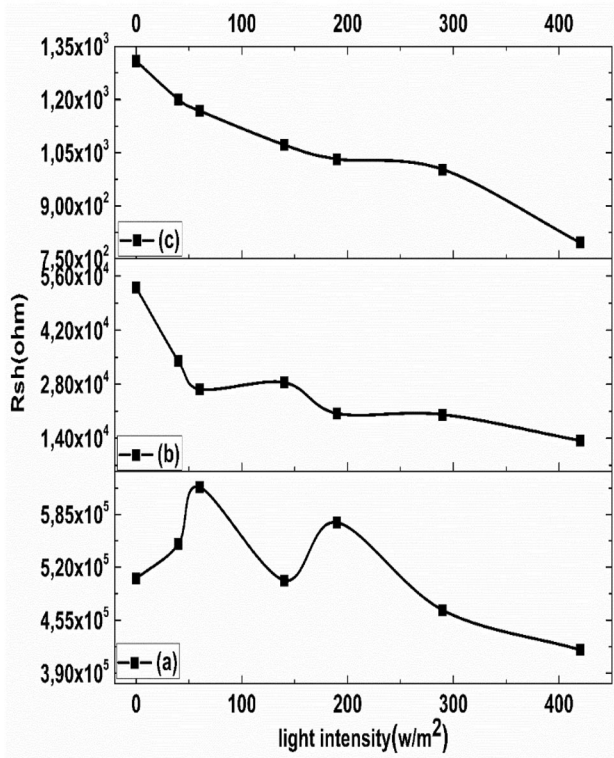
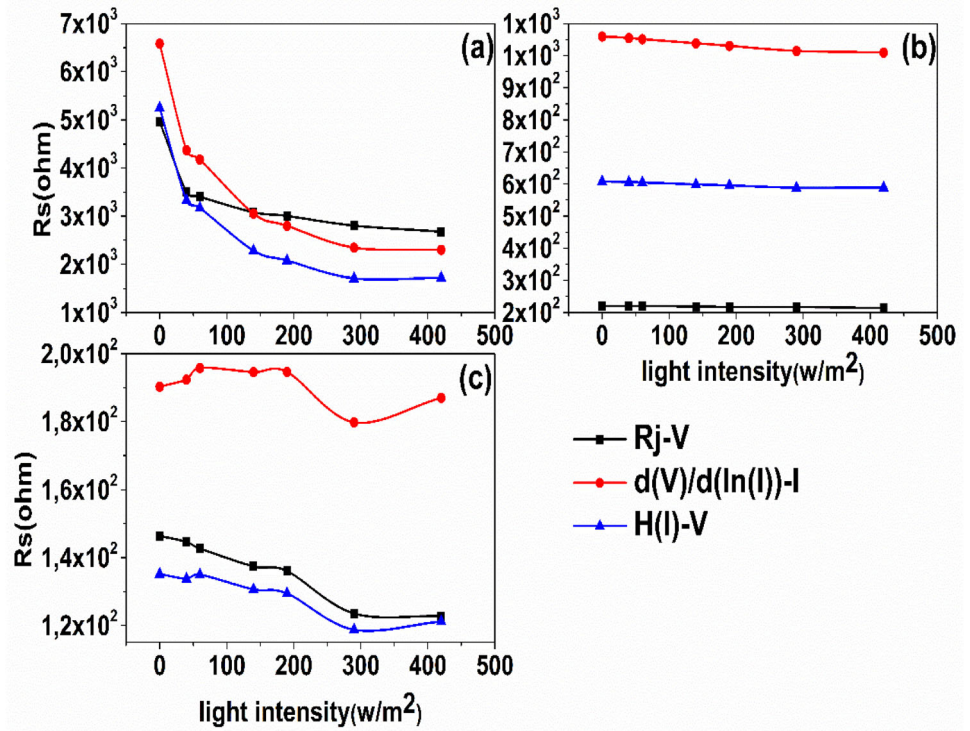


Fig. 9 Variation of R_{sh} values of heterojunction no: a 1st, b 2nd and c 3rd

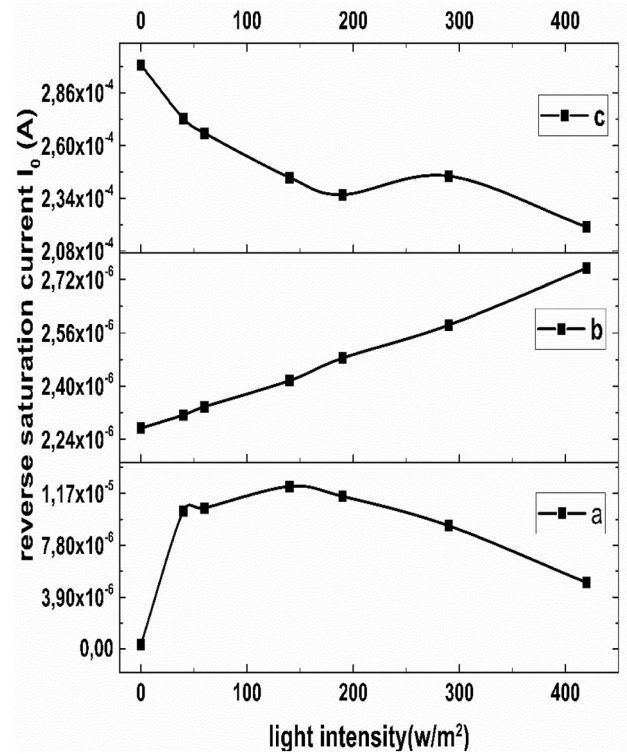


Fig. 10 Variation of I_0 values of heterojunction under light intensity: a 1st, b 2nd and c 3rd

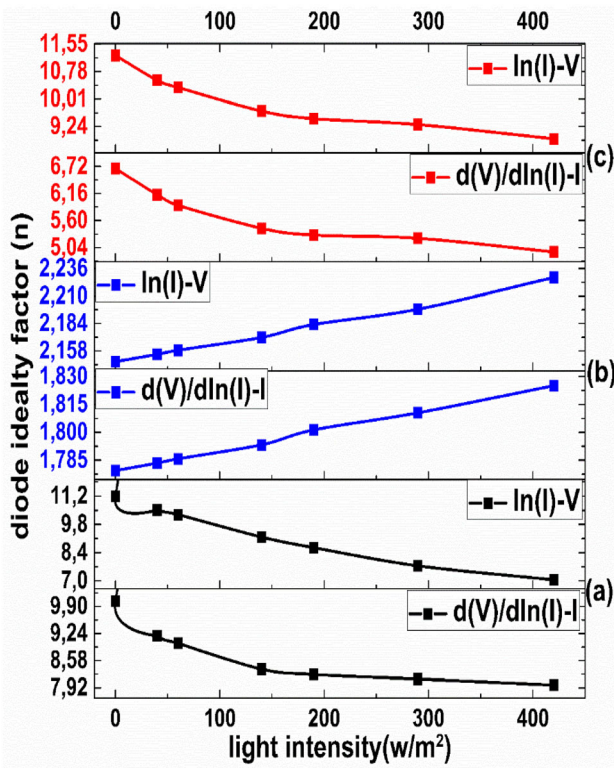


Fig. 11 Variation of n values of heterojunction according to light intensity: **a** 1st, **b** 2nd and **c** 3rd

possible reasons for this situation in the literature. These can be electron–hole generation–recombination state, depletion layer expansion, distribution of interfacial charges, inhomogeneity between TiO_2 and Si layer, and the effect of series resistance [29, 38].

According to Anderson’s model, Fig. 13a and b show energy–band diagram of p–Si/ TiO_2 heterojunction under equilibrium (dark conditions) and light conditions, respectively [39–41]. Band energies of TiO_2 vs p–Si are obtained as 3.2 vs 1.12 eV, respectively [41]. Electron affinities are calculated as $\chi(\text{TiO}_2) = 4.10$ eV [40] and $\chi(\text{Si}) = 4.05$ eV [19], respectively. Valence band offset (ΔE_v) and conduction band offset (ΔE_c) can be determined as $\Delta E_v = E_{g, \text{TiO}_2} - E_{g, \text{Si}} + \Delta E_c = 2.13$ eV and $\Delta E_c = \chi(\text{TiO}_2) - \chi(\text{Si}) = 0.05$ eV, respectively [41]. As a result of this, the holes are not easily injected from TiO_2 to n–type Si since valence band offset is greater than conduction band offset. However, free electrons migrate from p–type Si to TiO_2 owing to the existence of low potential energy barrier. Thus, they contribute majorly photo-generated current.

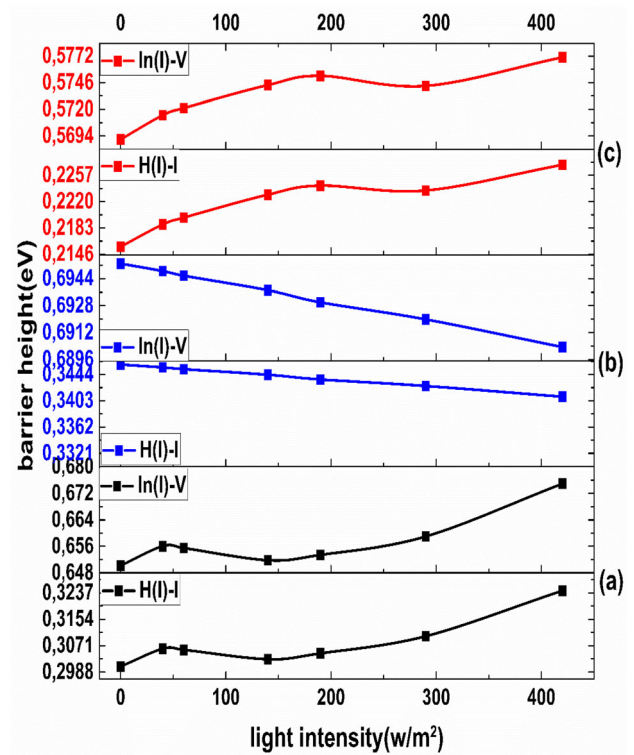


Fig. 12 Variation of ϕ_b values of heterojunctions according to light intensity **a** 1st, **b** 2nd and **c** 3rd

4 Conclusion

In this study, Ti metal was coated on p–type Si wafer surface by PVD Sputter process method. And then, a TiO_2 semiconductor films were produced with anodic oxidation at different potentials. Al/Si/ TiO_2 /Ag heterojunctions were produced for electrical characterization. The surface structures are rough and oxygen and titanium structure was homogeneously distributed through the surface. The electrical characterization of heterojunctions produced at different voltages was investigated in the ± 5 V potential range under dark and 40, 60, 140, 190, 290 and 420 W m^{-2} light intensity. All three heterojunctions showed rectifying properties and exhibited typical photo-sensitive photodiode behavior. R_s and R_{sh} values decreased with increasing light intensity. Minimum R_s and R_{sh} values were observed at the third heterojunction. While the n values of the 1st and 3rd heterojunctions decreased with increasing light intensity, the ϕ_b values increased. In 2nd heterojunction, the opposite behavior was observed. The minimum values were observed at 2nd heterojunction, while the minimum ϕ_b was observed at 1st

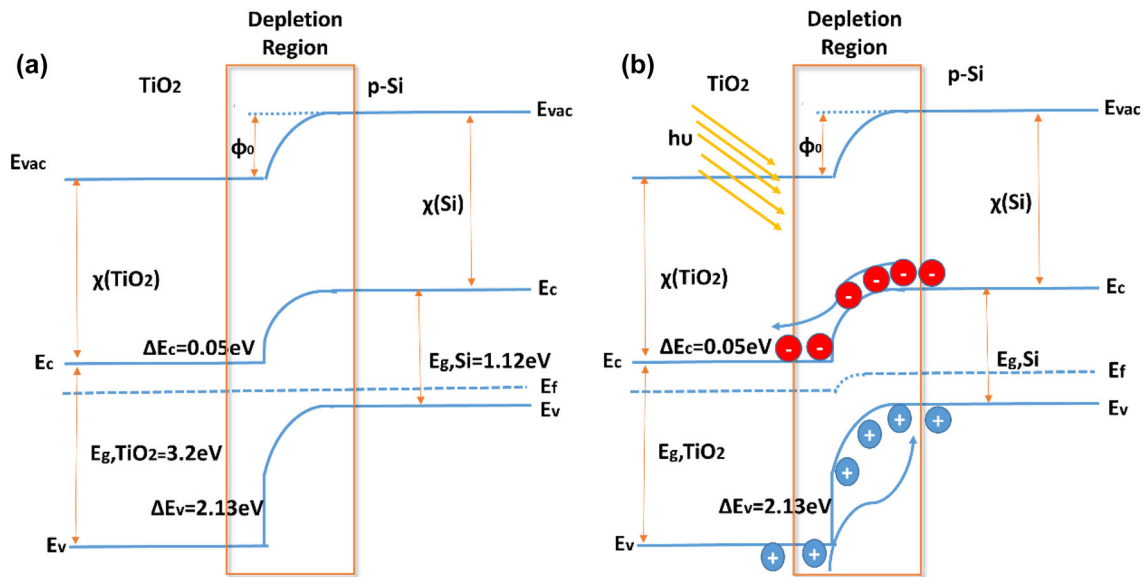


Fig. 13 Schematic energy-band diagram of TiO₂/p-Si heterojunction diode under equilibrium (dark conditions) and light conditions

heterojunction. While I_0 values of 1st heterojunction decreased with the light intensity, they increased in 2nd heterojunction. In 3rd heterojunction, it increased up to a certain light intensity and then decreased.

Acknowledgements

The authors would like to specially thank Mr. I. Irende for running SEM and EDX analyses at Ordu University – ODUMARAL.

Author contributions

FU: Conceptualization, Formal analysis, Investigation, Methodology, Project administration, Resources, Software, Validation, Visualization, Writing-draft, Writing-review & editing. MŞK: Investigation, Methodology, Resources, Visualization, Writing-original draft, Writing-review & editing. SD: Investigation, Methodology, Resources, Supervision, Validation, Visualization, Writing-original draft, Writing-review & editing.

Funding

There is no funding for this work.

Data availability

All data generated or analyzed during this study are included in this published article.

Declarations

Conflict of interest The authors declare the following financial interests/personal relationships that may be considered as potential competing interests.

References

1. F. Yakuphanoglu, Nanocluster n-CdO thin film by sol-gel for solar cell applications. *Appl. Surf. Sci.* **257**(5), 1413–1419 (2010)
2. M. Soyly et al., Photoelectrical characterization of a new generation diode having GaFeO₃ interlayer. *Sol. Energy Mater. Sol. Cells* **124**, 180–185 (2014)
3. H. Huang et al., Photoelectrochromic properties and energy storage of TiO_{2-x}N_x/NiO bilayer thin films. *Sol. Energy Mater. Sol. Cells* **94**(2), 355–359 (2010)
4. M. Cavas et al., Fabrication and electrical characterization of solution-processed all-oxide transparent NiO/TiO₂ p-n junction diode by sol-gel spin coating method. *J. Electroceram.* **31**(1–2), 260–264 (2013)
5. K. Mensah-Darkwa et al., Dye based photodiodes for solar energy applications. *Appl. Phys. A* **123**(10), 622 (2017)
6. S. Mansouri et al., Graphene oxide/poly (3-hexylthiophene) nanocomposite thin-film phototransistor for logic circuit applications. *J. Electron. Mater.* **47**(4), 2461–2467 (2018)

7. M. Zurnaci et al., Synthesis of a new 1,3,4-thiadiazole-substituted phenanthroimidazole derivative, its growth on glass/ITO as a thin film and analysis of some surface and optoelectronic properties. *New J. Chem.* **45**(48), 22678–22690 (2021)
8. Ünal, F., *ITO cam üzerine büyüdülen InSe/rubrene, CIS/rubrene, CIGS/rubrene, InSe/coronene, CIS/coronene, CIGS/coronene heteroeklemlerin yapısal, optik ve elektriksel özelliklerinin belirlenmesi.* 2021.
9. F. Unal, S. Demir, H. Mammadov, Structural, surface morphological, optical and electrical properties of InxSey thin films, an absorber layer for photovoltaic cells fabricated by M-CBD method using different variables. *Turk. J. Chem.* **45**(6), 1761–1773 (2021)
10. B. Coskun et al., Investigation of structural and electrical properties of Zirconium dioxide thin films deposited by reactive RF sputtering technique. *Ferroelectrics* **502**(1), 147–158 (2016)
11. F. Al-Hazmi, F. Yakuphanoglu, Cu₂ZnSnS₄: graphene oxide nanocomposites based photoresponse devices. *J. Alloy. Compd.* **653**, 561–569 (2015)
12. P. Roy, S. Berger, P. Schmuki, TiO₂ nanotubes: synthesis and applications. *Angew. Chem. Int. Ed.* **50**(13), 2904–2939 (2011)
13. C.A. Grimes, Synthesis and application of highly ordered arrays of TiO₂ nanotubes. *J. Mater. Chem.* **17**(15), 1451–1457 (2007)
14. A. Ghicov, P. Schmuki, Self-ordering electrochemistry: a review on growth and functionality of TiO₂ nanotubes and other self-aligned MO_x structures. *Chem. Commun.* **20**, 2791–2808 (2009)
15. F. Yakuphanoglu, Transparent metal oxide films based sensors for solar tracking applications. *Composite B* **92**, 151–159 (2016)
16. A.A. Hendi, F. Yakuphanoglu, Graphene doped TiO₂/p-silicon heterojunction photodiode. *J. Alloy. Compd.* **665**, 418–427 (2016)
17. N. Aslan et al., Ti doped amorphous carbon (Al/Ti-a: C/p-Si/Al) photodiodes for optoelectronic applications. *J. Mol. Struct.* **1155**, 813–818 (2018)
18. G. Rawat et al., Electrical and ultraviolet-A detection properties of E-beam evaporated n-TiO₂ capped p-Si nanowires heterojunction photodiodes. *IEEE Trans. Nanotechnol.* **16**(1), 49–57 (2017)
19. G. Rawat et al., Ultraviolet detection properties of p-Si/n-TiO₂ heterojunction photodiodes grown by electron-beam evaporation and sol–gel methods: a comparative study. *IEEE Trans. Nanotechnol.* **15**(2), 193–200 (2016)
20. S.R. Sani, Analysis of optoelectronic properties of TiO₂ nanowires/Si heterojunction arrays. *Chin. Phys. B* **23**(10), 1–10 (2014)
21. S.M. Kumbhar et al., Dip coated TiO₂ based metal-semiconductor-metal ultraviolet photodetector for UV A monitoring. *Superlatt. Microstruct.* **141**, 106490 (2020)
22. A. Kumar et al., Structural and electrical properties of Ag/n-TiO₂/p-Si/Al heterostructure fabricated by pulsed laser deposition technique. *J. Electron. Mater.* **46**(11), 6422–6429 (2017)
23. G. Rawat et al., Effective Richardson constant of sol-gel derived TiO₂ films in n-TiO₂/p-Si heterojunctions. *IEEE Electron Device Lett.* **38**(5), 633–636 (2017)
24. Cimilli Çatır, F.E., *Cu/n-InP/In SCHOTTKY DİYO-TLARIN SICAKLIĞA BAĞLI AKIM-VOLTAJ VE KAPASİTE-VOLTAJ ÖLÇÜMLERİNDEN ELDE EDİLEN KARAKTERİSTİK PARAMETRELERİNİN İNCELENMESİ.* Erzincan Üniversitesi Fen Bilimleri Enstitüsü Dergisi, 2018.
25. Rangel-Kuoppa, V.-T., et al., *Temperature dependence of current–voltage characteristics of Pt/InN Schottky barrier diodes.* 2010. pp. 53–54.
26. H.M.J. Al-Taii, V. Periasamy, Y.M. Amin, Electronic characterization of Au/DNA/ITO metal–semiconductor–metal diode and its application as a radiation sensor. *PLoS ONE* **11**(1), 423 (2016)
27. F. Yakuphanoglu, Photovoltaic properties of the organic–inorganic photodiode based on polymer and fullerene blend for optical sensors. *Sens. Actuators A* **141**(2), 383–389 (2008)
28. T.U. Kampen, S. Park, D.R.T. Zahn, Barrier height engineering of Ag/GaAs(100) Schottky contacts by a thin organic interlayer. *Appl. Surf. Sci.* **190**(1), 461–466 (2002)
29. E.H. Roderick, Metal-semiconductor contacts. *IEE Proc. I-Solid-State Electron Devices* **129**(1), 1 (1982)
30. E.H. Nicollian, J.R. Brews, *MOS (Metal Oxide Semiconductor) Physics and Technology* (Wiley, Hoboken, 2002)
31. Ş Altındal, Ö. Sevgili, Y. Azizian-Kalandaragh, A comparison of electrical parameters of Au/n-Si and Au/(CoSO₄-PVP)/n-Si structures (SBDs) to determine the effect of (CoSO₄-PVP) organic interlayer at room temperature. *J. Mater. Sci.* **30**(10), 9273–9280 (2019)
32. Thermometry, P.T., *Measurement science conference tutorial thermometry–fundamentals and practice.* 1993.
33. B. Gündüz et al., The photo-electrical properties of the p-Si/Fe(II)–polymeric complex/Au diode. *Synth. Met.* **184**, 73–82 (2013)
34. S.K. Cheung, N.W. Cheung, Extraction of Schottky diode parameters from forward current–voltage characteristics. *Appl. Phys. Lett.* **49**(2), 85–87 (1986)

35. H.G. Çetinkaya et al., Photovoltaic characteristics of Au/PVA (Bi-doped)/n-Si Schottky barrier diodes (SBDs) at various temperatures. *Curr. Appl. Phys.* **13**(6), 1150–1156 (2013)
36. H.E. Lapa et al., Effect of illumination on electrical parameters of Au/(P3DMTFT)/n-GaAs Schottky barrier diodes. *Indian J. Phys.* **94**(12), 1901–1908 (2020)
37. Ş Altındal et al., Electrical and photovoltaic properties of Au/(Ni, Zn)-doped PVA/n-Si structures in dark and under 250 W illumination level. *Mater. Sci. Semicond. Process.* **28**, 48–53 (2014)
38. S.S. Li, *Semiconductor Physical Electronics* (Springer, New York, 2012)
39. S. Aksoy, Y. Caglar, Structural transformations of TiO₂ films with deposition temperature and electrical properties of nanostructure n-TiO₂/p-Si heterojunction diode. *J. Alloy. Compd.* **613**, 330–337 (2014)
40. J.-Z. Chen et al., Preparation and characterization of surface photocatalytic activity with NiO/TiO₂ nanocomposite structure. *Materials* **8**(7), 4273–4286 (2015)
41. A. Dewasi, A. Mitra, Effect of variation of thickness of TiO₂ on the photovoltaic performance of n-TiO₂/p-Si heterostructure. *J. Mater. Sci.* **28**(23), 18075–18084 (2017)

Publisher's Note Springer Nature remains neutral with regard to jurisdictional claims in published maps and institutional affiliations.